Medical Engineering and Physics 43 (2017) 71–76

Contents lists available at ScienceDirect

Medical Engineering and Physics

journal homepage: www.elsevier.com/locate/medengphy

Effect of vibration frequency on biopsy needle insertion force

Lei Tan[a,c], Xuemei Qin[b], Qinhe Zhang[a,c,*], Hongcai Zhang[a,c], Hongjian Dong[a,c], Tuodang Guo[a,c], Guowei Liu[a,c]

[a] School of Mechanical Engineering, Shandong University, Jinan 250061, China
[b] Cancer Prevention Center, Qilu Hospital of Shandong University, Jinan 250061, China
[c] Key Laboratory of High Efficiency and Clean Mechanical Manufacture of Ministry of Education, Shandong University, Jinan 250061, China

ARTICLE INFO

Article history:
Received 10 March 2016
Revised 23 January 2017
Accepted 12 February 2017

Keywords:
Needle insertion
Vibration
Voigt model
Insertion force

ABSTRACT

Needle insertion is critical in many clinical medicine procedures, such as biopsy, brachytherapy, and injection therapy. A platform with two degrees of freedom was set up to study the effect of vibration frequency on needle insertion force. The gel phantom deformation at the needle cutting edge and the Voigt model are utilized to develop a dynamic model to explain the relationship between the insertion force and needle-tip velocity. The accuracy of this model was verified by performing needle insertions into phantom gel. The effect of vibration on insertion force can be explained as the vibration increasing the needle-tip velocity and subsequently increasing the insertion force. In a series of needle insertion experiments with different vibration frequencies, the peak forces were selected for comparison to explore the effect of vibration frequency on needle insertion force. The experimental results indicate that the insertion force at 500 Hz increases up to 17.9% compared with the force at 50 Hz.

1. Introduction

Needle insertion is a critical procedure in clinical medicine, and it is widely used in the diagnosis and therapeutics of prostate cancer. Needle insertion force is the subject of much research [1]. The force data are used for distinguishing between different tissue layers when the needle is inserted into tissue or for path planning in practice. The force has a relationship with the tissue deformation and needle deflection. Studies have shown that the axial force of a needle during insertion is the summation of different forces distributed along the needle shaft, such as stiffness force, frictional force, and cutting force. Some studies have modelled these forces [2].

As research on biopsy needles progresses, new types of biopsy needle are designed, and various methods for needle insertion are studied, such as rotating needle insertion, high-speed needle insertion, and vibratory needle insertion [3–5]. The insertion forces in these procedures have been studied [6]. The vibratory cutting used in traditional processes contributes to several advantages, such as better surface finish and reduced cutting force. In previous research on vibratory needle insertion, piezoelectric elements were used to vibrate the needle at high frequency and thereby reduced the friction force between the needle and tissue [7]. Barnett et al. designed experiments to test the insertion force of hypodermic needles through porcine skin at a wide range of frequencies and amplitudes using various needle diameters and a constant insertion velocity of 1 mm/s [8]. Begg and Slocum advanced the needle into tissue using a hypodermic needle with axial vibration. The results indicate that a lower insertion force is obtained at the correct frequency and that immediate tissue damage is reduced compared with insertions using ultrasonic vibration [9]. Vibratory fascicle insertion into human skin is also a common phenomenon. Mosquitos' special vibratory insertion skill contributes to an insertion force that is three orders of magnitude smaller than the lowest reported insertion force for an artificial micro-needle with an ultra-sharp tip [10]. However, there has been little research on the model of the relationship between vibration and needle force.

In this paper, the gel phantom deformation along the needle cutting edge and the Voigt model are used to develop a dynamic model to explain the relationship between the insertion force and needle-tip velocity. This model is utilized to explain the effect of vibration needle insertion on insertion force. Puncture experiments with different insertion velocities were performed to confirm this model. Needle insertion experiments with different vibration frequencies were also conducted to explore the effect of vibration frequency on needle insertion force.

* Corresponding author at: School of Mechanical Engineering, Shandong University, Jinan 250061, China.
E-mail address: zhangqh@sdu.edu.cn (Q. Zhang).

http://dx.doi.org/10.1016/j.medengphy.2017.02.011
1350-4533/

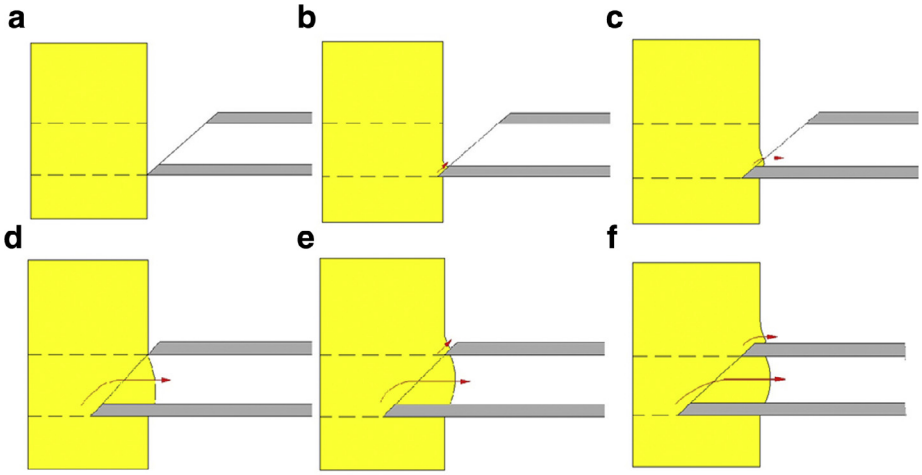

Fig. 1. Gel phantom deformation along with cutting edge.

2. Force model

2.1. Relationship between insertion force and needle-tip velocity

There has been a great deal of research on needle insertion force. The most common modelling method divides the needle force into three parts: stiffness force, friction force, and tip force [11]. The stiffness force is a resistance force generated when the organ membrane prevents tissue from being punctured by a needle. There is no skin covering the gel phantom to be punctured, and the needle is easily inserted into the gel phantom without obvious contact force. Therefore, the stiffness force is neglected during needle insertion in this paper. The needle force model when a needle is inserted into a gel phantom can be described as follows:

$$F_{insertion} = F_{friction} + F_{tip} \tag{1}$$

The friction force along the needle surface is caused by interaction between the needle and the tissue. Needle insertion into gel phantom causes the deformation and compression of the phantom. This deformation and compression of the gel phantom generates a force that acts on the needle perpendicular to the needle's surface. This force could be modelled by a modified Winkler's foundation [12]:

$$F_n = \xi L\Lambda = \frac{\beta E_2}{1-\upsilon^2}\left[\frac{E_2 b^4}{E_1 I_n(1-\upsilon^2)}\right]^{\gamma} \cdot \mathrm{L} \cdot \frac{D}{2} \tag{2}$$

where F_n is the force along the needle shaft as a result of tissue deformation and compression, ξ is the foundation modulus, L is the contact length, and Λ refers to half the diametrical interference ($D/2$). β and γ are working condition coefficients. E_1 and I_n are Young's modulus and moment of inertia of the needle, respectively. υ is the Poisson ratio of soft tissue, and b is the function width, which is simplified using $b = \pi D$.

The friction force along the needle surface is generated as a result of sliding between the needle surface and the gel phantom and can be calculated as

$$F_{friction} = \mu F_n \tag{3}$$

where μ is the dynamic friction coefficient between the needle surface and the tissue.

The tip force is the force acting on the needle's cutting edge. The procedure of needle insertion into gel phantom is shown in Fig. 1. In Fig. 1(a), the needle begins to contact the gel phantom. Similar to the chip formation process in the mechanism of metal cutting, Fig. 1(b) shows that the gel phantom deforms along the needle cutting edge. The soft gel phantom enters into hollow needle instead of forming a chip, as shown in Fig. 1(c). The soft gel phantom enters into the hollow needle as shown in Fig. 1(d)–(f).

As shown in Fig. 2, gel phantom deformation occurs at the cutting edge of the needle tip because of needle insertion. The gel phantom is divided into element layers in Fig. 2(a). The deformation can be considered as the sum of the deformation of the element layers. The element layer nearest the cutting edge is taken out to analyse the deformation, strain, and strain rate [13]. Fig. 2(b) shows that the COAB in the element layer transforms into the OAFE when the cutting edge moves from point C to point O. The strain

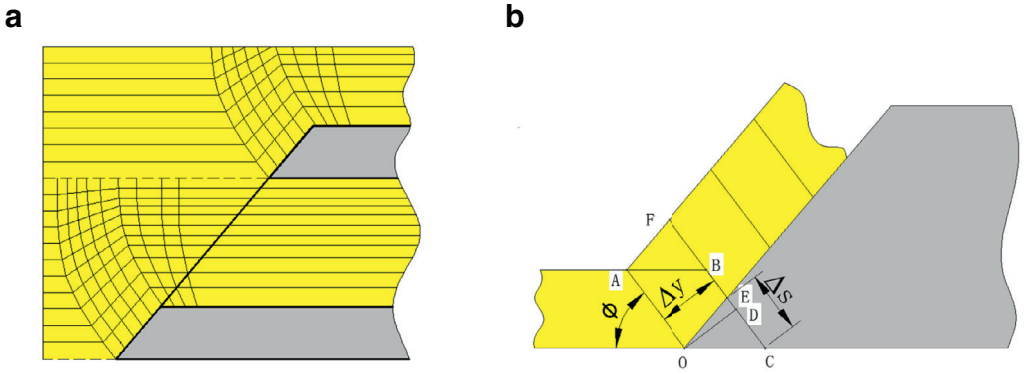

Fig. 2. Gel phantom deformation along needle cutting edge: (a) gel phantom deformation grid. (b) Shearing strain of gel phantom at cutting edge.

and the strain rate are expressed as follows:

$$\varepsilon = \frac{\Delta s}{\Delta y} = \cot(\phi - \gamma_0) \tag{4}$$

$$\dot{\varepsilon} = \frac{\varepsilon}{\Delta t} = \frac{\Delta s}{\Delta y \Delta t} = \frac{\varepsilon v \sin\phi}{\Delta y} \tag{5}$$

where ε, $\dot{\varepsilon}$ and ϕ are the strain, strain rate, and shear angle of the gel phantom, v and γ_0 are the insertion velocity and the rake angle of the needle tip, respectively. Needle insertion is a sequential procedure, and the gel phantom is treated as a sequential and homogeneous viscoelastic body. Based on continuum mechanics, when Δt becomes infinitesimal, the strain rate can be expressed as follows:

$$\dot{\varepsilon} = \frac{\varepsilon}{\Delta t} = \frac{d\varepsilon}{dt} \tag{6}$$

The internal stress of the gel phantom is generated due to deformation. Because of the viscoelastic property of the gel phantom, the Voigt model can be utilized and expressed as follows:

$$\sigma = E\varepsilon + \eta \frac{d\varepsilon}{dt} \tag{7}$$

where σ is the stress of the gel phantom, E is the elasticity modulus, and η is the viscosity coefficient of the gel phantom [14].

As stated in Newton's third law, a force acts along with the needle's axial direction due to the stress of the gel phantom:

$$F_{tip} \propto \sigma(v) \tag{8}$$

As seen from Eq. (8), the increasing trend in needle-tip force is related to the increase in strain rate. Substituting Eqs. (2) and (3) into Eq. (1), allows the total insertion force to be given as follows:

$$F_{insertion} = \frac{\mu L D}{2} \cdot \frac{\beta E_2}{1-\upsilon_2^2} \left[\frac{E_2 (\pi D)^4}{E_1 I_n (1-\upsilon_2^2)} \right]^{\gamma} + F_{tip} \tag{9}$$

Judging from Eq. (9), the insertion force has a positive correlation with needle-tip velocity at the same insertion depth. Experiments were designed to confirm this law at insertion velocities of 1 mm/s, 10 mm/s, and 100 mm/s.

2.2. Relationship between needle-tip velocity and vibration velocity

During the vibratory needle insertion procedure, the needle-tip velocity, $v_t(t)$, is composed of two components and can be expressed as follows:

$$v_t(t) = v_v(t) + v_i(t) \tag{10}$$

where $v_i(t)$ is the motor insertion velocity, and $v_v(t)$ is the vibratory velocity.

The vibratory velocity of a needle tip can be determined by taking the derivative of the sinusoidal amplitude, as follows:

$$v_v(t) = 2\pi f A \cos(2\pi f t) \tag{11}$$

where f is the vibration frequency and A is amplitude of the needle tip.

Needle insertion experiments with different vibration frequencies were performed to explore the effect of frequency on insertion force.

3. Materials and methods

Two experimental procedures were performed to confirm the model and explore the effect of vibration frequency on insertion force. In the first procedure, the needle was inserted into the gel phantom at velocities of 1 mm/s, 10 mm/s, and 100 mm/s. In the second procedure, the needle was inserted into the gel phantom at a vibration amplitude of 1 μm, an insertion velocity of 10 mm/s, and vibration frequencies of 50, 100, 150, 250, and 500 Hz. All experiments with the same parameters were repeated five times to gather force data.

3.1. Experimental platform

The platform shown in Fig. 3, set up to study the insertion force during the needle insertion into the gel phantom, provided two degrees of freedom. The linear motor provided a horizontal linear motion with a maximum stroke of 270 mm. The linear motor consists of three parts: the slider, coil, and controller. The drive system is a P01-23SX80 / 210 × 270 model linear-motor drive system (Linmot Co., US). The slider stroke and speed are controlled through custom software. The *X*–*Y* cross slippery platform permitted movement in both directions on a horizontal plane. The maximum stroke of the *X*–*Y* cross slippery platform is 200 mm, and the repeatability positioning accuracy is 5 µm. The container holding the gel phantom was fixed on the *X*–*Y* cross slippery platform.

3.2. Experimental needle and phantom

The biopsy needle used in these experiments was a 16 cm, 18 G, 20° bevel-tip, hollow needle. The phantom used in these experiments was a gel phantom that exhibits elastic and viscoelasticity properties similar to those of soft tissue in force measurements [15]. A gel phantom is more suitable than soft tissue for studying the insertion force because of its homogeneous, isotropic property. The gel phantom can also be given different values for Young's modulus and the Poisson ratio by altering its composition [16]. The gel phantom used in this paper is a mixture of 12% gelatine and

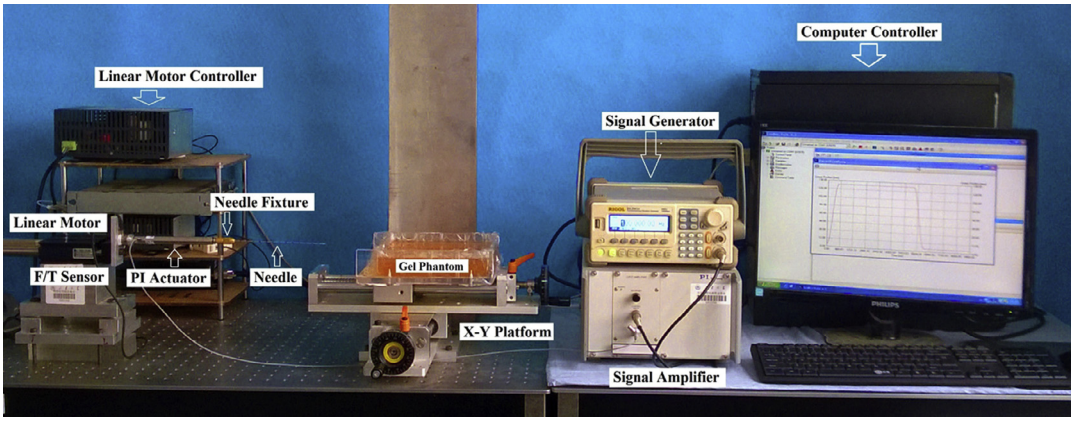

Fig. 3. Experimental platform.

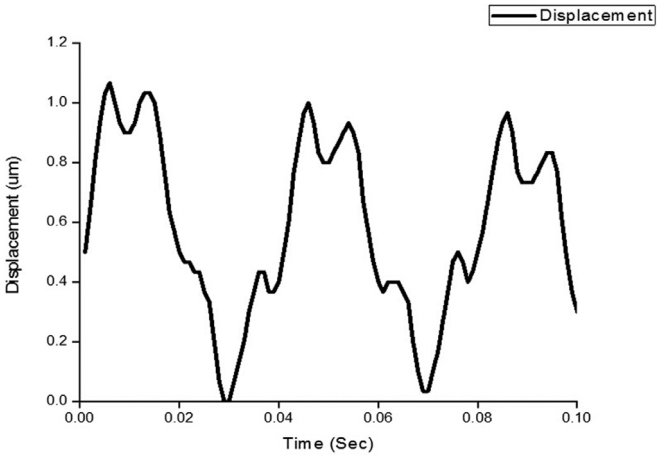

Fig. 4. Vibration amplitude.

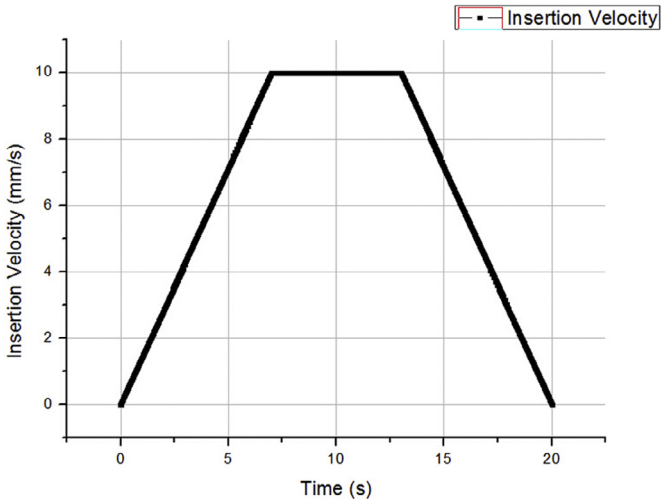

Fig. 5. Insertion velocity about time.

water. The gelatine was dissolved in hot water by stirring it. After dissolving, the gel phantom was allowed to cool down at room temperature for 16 h.

3.3. Force measurements

A 6-DOF force/torque sensor was used to measure the forces and torques when the needle was inserted into the gel phantom. The force sensor used was an ATI nano 17 SN-25-0.25 with a range of 25 N and a theoretical accuracy of 6.25 mN. The analogue signal from the force/torque sensor was converted into a digital signal by DAQ Card with a sample rate of 60 Hz.

3.4. Vibration method

Needle vibration was generated by a preloaded piezo actuator connected to the needle. A sinusoidal alternating voltage signal was generated from 0–10 V by a signal generator (DG 2041A, RiGol, China). The signal was set to act on the preloaded piezo actuator after 10x voltage amplification by a voltage amplifier (E505, Physik Instrumente, Germany). The preloaded piezo actuator (P-840.60, Physik Instrumente, Germany) would then provide a sinusoidal vibration to the needle under the effect of the sinusoidal alternating voltage signal. The preloaded piezo actuator's vibration amplitude varied from 0 to 90 μm when the voltage signal was changed from 0 to 100 V. The vibration amplitude of the needle tip was measured by a laser displacement sensor (LK-G30, KEYENCE, Japan). As shown in Fig. 4, the vibration on needle tip was approximately sinusoidal. In this paper, the vibration amplitude was maintained at 1 μm, and the vibration frequency was varied from 50 to 500 Hz. According to Eq. (11), the maximum vibration velocity varied from 0.314 to 3.14 mm/s when the vibration frequency was changed from 50 to 500 Hz.

3.5. Needle insertion method

The needle insertion velocity was provided by the linear motor. Through the custom software, the insertion velocity over time was generated automatically after inputting the speed and insertion distance. The needle tip was 50 mm from the gel phantom at the starting position. In the first procedure, the insertion speed was reached and maintained at velocities of 1 mm/s, 10 mm/s, and 100 mm/s before the needle was inserted into the gel phantom. During the second procedure, the velocity of the linear motor was increased to 10 mm/s from 0 s to 7 s, kept at 10 mm/s from 7 s to 13 s, and decreased to 0 mm/s from 13 s to 20 s, as shown in Fig. 5. The needle tip reached the gel phantom at a time of 8.5 s and a speed of 10 mm/s, and the needle insertion depth was 45 mm at 13 s.

4. Results and discussion

4.1. Effect of needle insertion velocity on needle insertion force

The insertion forces were measured when the needle was inserted into gel phantom at three different velocities: 1 mm/s, 10 mm/s, and 100 mm/s. As seen in Fig. 6(a), the insertion force increases with the insertion depth at each of the three velocities. The comparison of insertion force at the insertion depth of 80 mm is shown in Fig. 6(b). There is a close relationship between the insertion force and the insertion velocity: the insertion force is proportional to the insertion velocity at the same insertion depth. The strain rate of the deformed gel phantom increases with increasing insertion velocity at the same insertion depth. This contributes to a larger stress in the gel phantom and a greater reactive force on the needle tip. These results align well with the results of Eq. (9), and this relationship has been shown in previous research results [17].

4.2. Effect of vibration on needle insertion force

In Fig. 7, the insertion forces are shown to increase with insertion depth at a constant vibration amplitude of 1 μm and vibration frequencies ranging from 50 to 500 Hz. Between the insertion depths of 0 and 45 mm, there is little difference between the needle tip velocities at different vibration frequencies. This is because the linear motor velocity is constant at 10 mm/s and the vibration speed is small; therefore, the slopes of the insertion forces at different frequencies are nearly the same.

As seen from Fig. 8, the linear motor insertion velocity decreases at the insertion depth of 45 mm. The maximum vibratory velocity is constant. Therefore, the proportion of vibration velocity in the needle-tip velocity increases after the linear motor speed decreases. The difference between needle-tip velocities under different vibration frequencies increases as the insertion depth increases. As a result, the slopes of the insertion forces at different frequencies become different at insertion depths from 45 mm to 80 mm, as seen in Fig. 7.

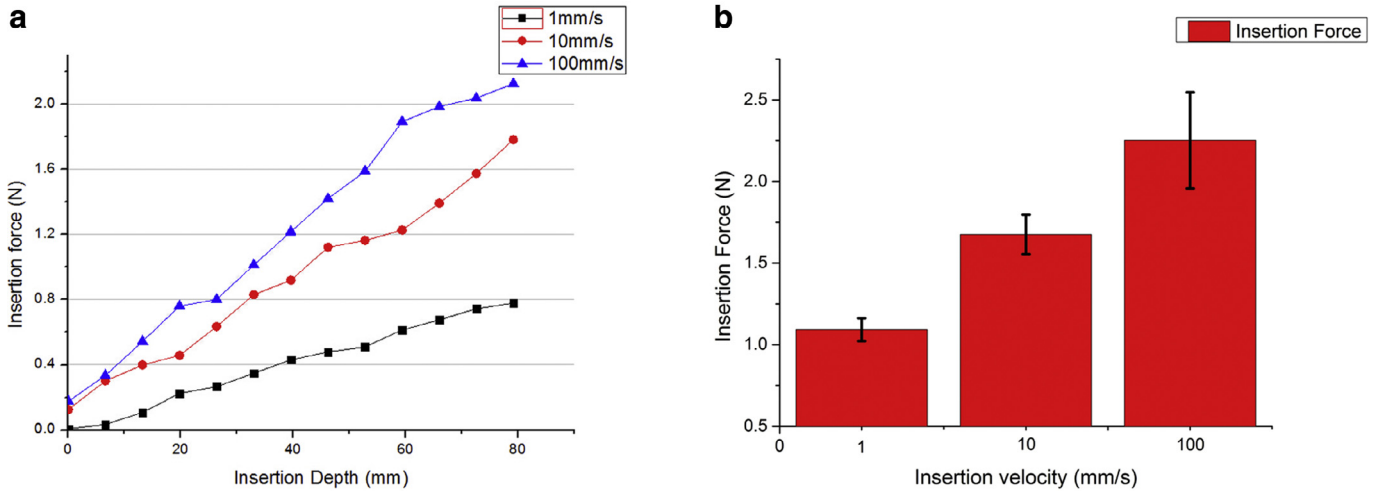

Fig. 6. Insertion force at different insertion velocity: (a) force throughout the insertion procedure. (b) Force at the insertion depth of 80 mm.

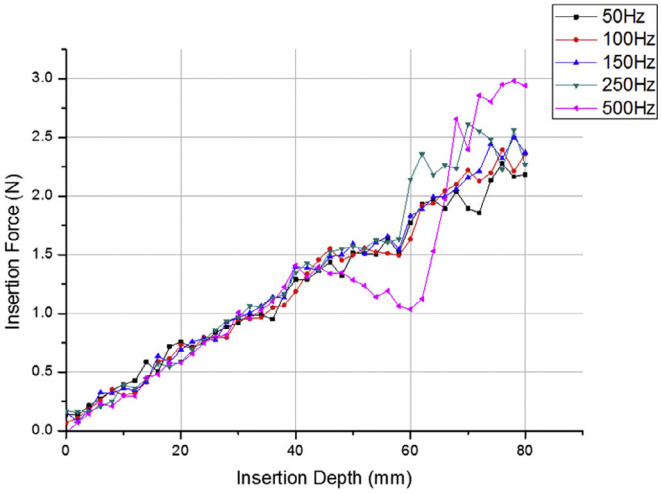

Fig. 7. Insertion force at different frequency.

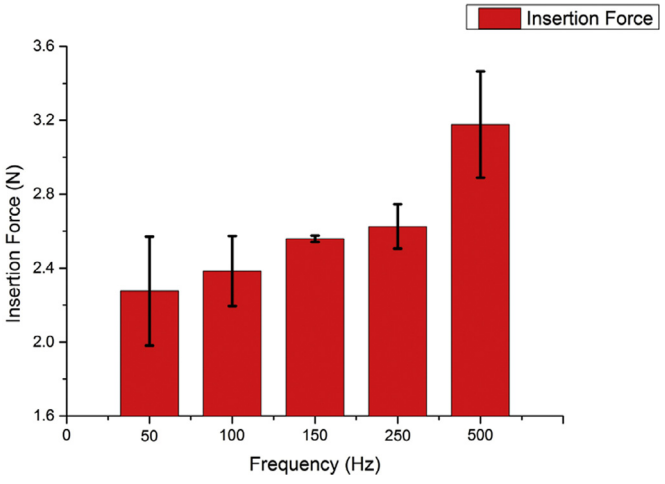

Fig. 9. Insertion force comparison at depth of 80 mm.

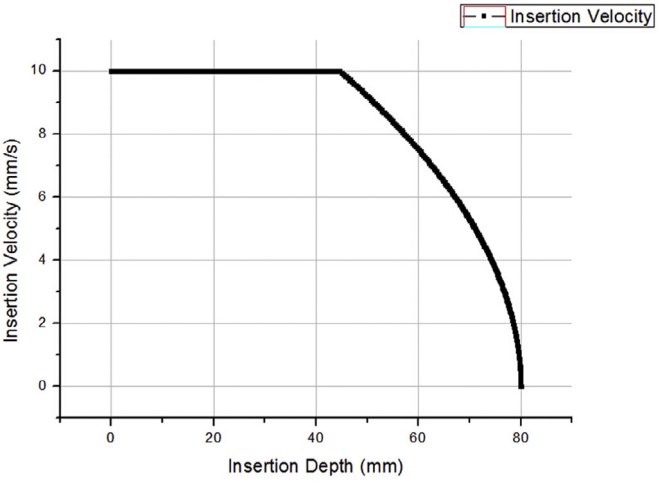

Fig. 8. Insertion velocity with insertion depth.

4.3. Comparison of insertion force at different vibration frequencies

As seen in Fig. 7, the insertion force increases with the insertion depth. Unlike animal organs, the surface of the gel phantom has no biological membrane. Therefore, the force increases smoothly without an obvious force decrease during the needle insertion procedure. Furthermore, due to the lack of a membrane on the gel phantom, it is difficult to determine the precise point when the needle punctures the surface of the gel phantom. The insertion forces reach a peak at the depth of 80 mm, where the motor velocity becomes zero and the vibration velocity is the only velocity. The measured forces at an insertion depth of 80 mm were selected for comparison in order to study the effect of vibration frequency on insertion force.

Fig. 9 shows that the insertion force increases with the vibration frequency when the vibration amplitude is held constant. The insertion force at 500 Hz shows an increase of up to 17.9% as compared to the force at 50 Hz. The results are consistent with the model presented in Section 2. It has been shown in similar research that the insertion force at the same depth decreases at a low frequency and increases at a high frequency [9]. The insertion force decreasing at narrow range of a low frequency is mainly due to the vibration reducing friction. In addition, the insertion force increasing at a high frequency is mainly due to the effect of high vibratory velocity on cutting tissues. As shown in Eq. (10), high vibratory velocity contributes to high needle-tip velocity when the motor insertion velocity is constant. According to Eq. (9), the needle insertion force becomes higher when the needle-tip velocity increases.

4. Conclusions and future research

Through studying the relationship between the insertion force and insertion velocity, the insertion force is proportional to the insertion velocity at the same insertion depth. Through applying vibration to a hollow needle, the insertion force along the surface of needle increases at the vibration amplitude of 1 μm and a range of vibration frequency from 50 to 500 Hz. The insertion force with 500 Hz vibration is 17.9% greater than the force with 50 Hz vibration. In the procedures of prostate biopsy and brachytherapy, the needle deflection is also a critical parameter. In future research, the effect of needle vibratory insertion on needle deflection will be explored.

Conflict of interest

None.

Ethical approval

Not required.

Acknowledgments

This work is supported by grants from The National Natural Science Foundation of China (Grant no. 51475274) and The Specialized Research Fund for the Doctoral Program of Higher Education (Grant no. 20130131110070).

References

[1] Abolhassani N, Patel R, Moallem M. Needle insertion into soft tissue: a survey. Med Eng Phys 2007;29:413–32.
[2] Simone C. Modeling of needle insertion forces for percutaneous therapies. M.S. thesis, Department of Mechanical Engineering, Hopkins University; MD. 2002.
[3] van de Berg NJ, Dankelman J, van den Dobbelsteen JJ. Design of an actively controlled steerable needle with tendon actuation and FBG-based shape sensing. Med Eng Phys 2015;37:617–22.
[4] Han P, Ehmann K. Study of the effect of cannula rotation on tissue cutting for needle biopsy. Med Eng Phys 2013;35:1584–90.
[5] Wolkowicz K, Moore JZ, McLaughlin. Novel pneumatic device for high speed needle insertion in brachytherapy. J Med Devices 2013;7:030945.
[6] van Gerwen DJ, Dankelman J, van den Dobbelsteen JJ. Needle–tissue interaction forces – a survey of experimental data. Med Eng Phys 2012;34:665–80.
[7] Huang YC, Tsai M, Lin C. A piezoelectric vibration-based syringe for reducing insertion force. In: Proceedings of the 2012 IOP conference series on materials science and engineering; 2012. p. 12020–3.
[8] Barnett AC, Wolkowicz K, Moore JZ. Vibrating needle cutting force. In: Proceedings of the 2014 international manufacturing science and engineering conference (ASME); 2014 V002T02A025.
[9] Begg NDM, Slocum AH. Audible frequency vibration of puncture-access medical devices. Med Eng Phys 2014;36:371–7.
[10] Kong X, Wu C. Measurement and prediction of insertion force for the mosquito fascicle penetrating into human skin. J Bionic Eng 2009;6:143–52.
[11] Okamura AM, Simone C, O'Leary MD. Force modeling for needle insertion into soft tissue. IEEE T Bio-Med Eng 2004;51:1707–16.
[12] Jiang S, Li P, Yu Y, et al. Experimental study of needle–tissue interaction forces: effect of needle geometries, insertion methods and tissue characteristics. J Biomech 2014;47:3344–53.
[13] Ai X. High-speed machining theoretical basis. High speed machining technology. Beijing: National Defense Industry Press; 2003. p. 21–55.
[14] Christensen R. Viscoelastic stress strain constitutive relations. Theory of viscoelasticity: an introduction. 2nd ed. New York: Academic Press; 1981. p. 16–20.
[15] DiMaio SP, Salcudean SE. Needle insertion modeling and simulation. IEEE Trans Robot Autom 2003;19:864–75.
[16] Meltsner MA, Ferrier NJ, Thomadsen BR. Observations on rotating needle insertions using a brachytherapy robot. Phys Med Biol 2007;52:6027–37.
[17] Crouch JR, Schneider CM, Wainer J, Okamura AM. A velocity-dependent model for needle insertion in soft tissue. In: Duncan JS, editor. Medical image computing and computer-assisted intervention (MICCAI), 3750. Berlin Heidelberg: Springer; 2005. p. 624–32.